Eliminating Potential Errors Caused by the Thin Shell Assumption: An Extended 3D UNB Ionospheric Modelling Technique

Wei Zhang[1], Richard B. Langley[1], Attila Komjathy[1,2], and Simon Banville[1,3]

[1]*Geodetic Research Laboratory, Department of Geodesy and Geomatics Engineering, University of New Brunswick, Fredericton, NB, Canada*

[2]*Jet Propulsion Laboratory / California Institute of Technology, Pasadena, CA, USA*

[3]*Geodetic Survey Division, Natural Resources Canada, Ottawa, ON, Canada*

BIOGRAPHY

Wei Zhang received his M.Sc. degree (2009) in space science from the School of Earth and Space Science of Peking University, China. He is currently a M.Sc.E. student in the Department of Geodesy and Geomatics Engineering at University of New Brunswick (UNB) under the supervision of Dr. Richard B. Langley. His research topic is the assessment of three-dimensional (3D) regional ionosphere tomographic models using global navigation satellite system (GNSS) measurements.

Richard B. Langley is a professor in the Department of Geodesy and Geomatics Engineering at UNB, where he has been teaching and conducting research since 1981. He has a B.Sc. in applied physics from the University of Waterloo and a Ph.D. in experimental space science from York University, Toronto. Prof. Langley has been active in the development of GPS error models since the early 1980s and has been a contributing editor and columnist for GPS World magazine since its inception. He is a fellow of The Institute of Navigation (ION), the Royal Institute of Navigation, and the International Association of Geodesy. He was a co-recipient of the ION Burka Award for 2003 and received the ION Johannes Kepler Award in 2007.

Attila Komjathy is a principal investigator of the Ionospheric and Atmospheric Remote Sensing (IARS) group at the Jet Propulsion Laboratory (JPL) and adjunct professor at UNB, specializing in remote sensing techniques using GPS. Prior to his joining JPL in July of 2001, he worked on the utilization of GPS reflected signals as a research associate at the University of Colorado's Center for Astrodynamics Research. He received his Ph.D. from the Department of Geodesy and Geomatics Engineering of UNB in 1997. He is a member of the WAAS Integrity and Performance Panel (WIPP).

Simon Banville is working for the Geodetic Survey Division (GSD) of Natural Resources Canada (NRCan) on real-time precise point positioning (PPP) using global navigation satellite systems. He is also in the process of completing his Ph.D. degree at the UNB under the supervision of Dr. Langley.

ABSTRACT

Ionospheric modelling has become an focus area within the global navigation satellite system (GNSS) community using several satellite-based augmentation systems (SBAS) (e.g., Wide Area Augmentation System (WAAS), European Geostationary Navigation Overlay Service (EGNOS), and MTSAT Satellite-based Augmentation System (MSAS)). Data-driven models have been applied with these systems and demonstrated as the best candidates for post-processing and other real-time applications due to their real-time applicability and relatively higher accuracy compared to empirical ionospheric modelling techniques.

In this paper, our objective is to improve the accuracy for the real-time positioning applications. To achieve this, we extended the University of New Brunswick-Ionospheric

Modelling Technique (UNB-IMT) from two-dimensions (2D) to three-dimensions (3D) by modelling the vertical dimension of the ionosphere using empirical orthogonal functions (EOFs) to eliminate the potential mapping function errors. The benefits of the new proposed modelling technique are demonstrated in a small regional network using post-fit residuals, estimated vertical total electron content (vTEC), as well as the repeatability of the estimates of differential code biases (DCBs). The ionospheric results from 3D UNB-IMT are also compared with those from widely-used 3D spherical harmonic (SH) models to show the beneficial effect of improving sensitivity owing to the effective and meaningful parameters in the model.

INTRODUCTION

Ionospheric modelling plays an important role in improving the accuracies of positioning and navigation, especially for current civil aircraft navigation and mass-market single-frequency users. Measurement-driven models are considered to be among the best candidates for real-time single-frequency positioning owing to their real-time applicability and relatively higher accuracy compared to empirical models, such as the GPS broadcast (also known as Klobuchar) and NeQuick models. A good example of a real-time positioning application is satellite-based augmentation systems (SBAS), such as Wide Area Augmentation System (WAAS), European Geostationary Navigation Overlay Service (EGNOS), and MSTAT Satellite-based Augmentation System (MSAS). Since the ionosphere can be the largest error source in single-frequency positioning, the accuracy of ionospheric modelling is critical for single-frequency applications.

Several organizations have been routinely providing ionospheric products to correct errors caused by the ionosphere in the form of ionospheric maps, i.e. vertical total electron content (vTEC) at grid points (including regional and global products), such as those from WAAS [*Sparks et al.*, 2011a,b] and the International GNSS Service (IGS) [*Feltens*, 2007; *Hernández-Pajares et al.*, 1999; *Mannucci et al.*, 1998; *Schaer et al.*, 1998], with various processing time delays ranging from near real time to a couple of weeks. Among the earliest works of ionosphere modelling, the University of New Brunswick-Ionospheric Modelling Technique (UNB-IMT) was developed in the mid-1990s [*Komjathy and Langley*, 1996a,b]. This technique was demonstrated for effectively deriving both regional and global total electron content (TEC) maps [*Komjathy*, 1997]. However, most of the models, including the current version of UNB-IMT, approximate the ionosphere using a single thin shell approach with an altitude set at e.g., 350 km, which may introduce additional modelling errors up to several TECU (1 TECU = 10^{16} electrons/m^2) [*Komjathy*, 1997] , corresponding to several metres of measurement delay or advance at the GPS L1 frequency.

To overcome any downside of such models, three-dimensional (3D) ionospheric tomographic modelling methods have been proposed [*Austen et al.*, 1988; *Howe et al.*, 1998] and implemented [*Gao and Liu*, 2002; *Hansen*, 1998; *Hernández-Pajares et al.*, 1999; *Lee et al.*, 2007; *Mitchell and Spencer*, 2003; *Schmidt et al.*, 2008; *Wen et al.*, 2007] by several groups since the late 1990s. Different from the two-dimensional (2D) single thin shell ionospheric models where the parameters to be estimated are TEC, the modelled variables in the tomographic model are related to electron density functions. Therefore, a more complex structure of electron densities (such as that observed during ionospheric storms or in the highly variable equatorial anomaly) may be expected to be revealed by the models. A commonly-accepted modelling approach is to describe the ionospheric horizontal (longitudinal and latitudinal) variability by a spherical harmonic (SH) expansion up to a specific degree and its vertical dimension modelled by empirical orthogonal functions (EOFs). The performance of such modelling approaches has been demonstrated by several research groups [*Gao and Liu*, 2002; *Hansen*, 1998; *Mitchell and Spencer*, 2003].

However, SH models are not ideal for capturing local variability in the ionosphere as each basis function of spherical harmonics exists over the entire geographic region of interest, such as the entire globe in the case of global modelling. In other words, localized measurements will have influence on the estimated state across the whole globe. As alternative approaches, wavelet [*Hansen*, 2002; *Schmidt et al.*, 2008] and finite element (meshes/pixels) [*Hernández-Pajares et al.*, 1999; *Lee et al.*, 2007; *Wen et al.*, 2007] models were proposed and implemented to capture the localized information content in the measurements and pass this information on to the end user. On the other hand, the inversion process can occasionally become singular as many of the parameters to be estimated tend to be ineffective and less meaningful. This is especially the case when our goal is to obtain better accuracies with higher order wavelet bases or smaller meshes/pixels. Due to the potential computing and transmitting burden, the two modelling techniques may have more difficulties associated with real-time applications, such as real-time single-frequency positioning, although they have advantages for capturing localized structures in

the ionosphere.

In this paper, aiming for potential real-time applications of 3D tomographic models, we extend the UNB-IMT from 2D to 3D by modelling the vertical dimension of the ionosphere using EOFs, and compare its performance with the 3D SH approach. The 2D UNB-IMT was demonstrated to work with various network sizes: regional, baseline by baseline, and even single standalone stations [*Komjathy*, 1997; *Rho et al.*, 2004]. Therefore, it is expected that this technique will help in capturing localized ionospheric structures above small regional networks or above a single standalone station compared to the 3D SH approach. Additional benefits may be expected for disturbed ionospheric conditions. For assessing the two modelling techniques, a small regional network was chosen to perform station-by-station and batch processes. The performance of both methods with the two processing scenarios is compared by analyzing the post-fit residuals and vTECs of the state estimation process, as well as the repeatability of estimates of differential code biases (DCBs) for both quiet and disturbed ionospheric conditions.

3D UNB-IMT

Due to the limited number of ionospheric parameters to be estimated, the 2D UNB-IMT was considered to be suitable for real-time applications (in fact, it can be proven that the modelling method of current 2D UNB-IMT is identical to the planar fit of WAAS in nature if the locations of reference stations tend to collocate with WAAS ionospheric grid points (IGPs)), such as real-time single-frequency precise point positioning (PPP) and SBASs [*Rho et al.*, 2005]. Therefore, for improving modelling accuracy for potential real-time applications, the 3D UNB-IMT modelling strategy will be introduced in this section and its applicability will be demonstrated with a regional network and single standalone stations.

1. Model Description

In order to clearly present the technique demonstrated in this research, we first briefly review the 2D UNB-IMT. Linear polynomial functions were initially proposed for describing the spatial variability of the ionosphere [*Komjathy*, 1997]. The model is expressed by the following equation:

$$TEC_r^s(t_p) = M(e_r^s)\cdot[a_{r,0}(t_p) + a_{r,1}(t_p)\cdot\triangle\lambda_r^s + a_{r,2}(t_p)\cdot\triangle\phi_r^s] + dcb_r + dcb^s \quad (1)$$

where

- $TEC_r^s(t_p)$: the ionospheric slant TEC (TECU, where 1 TECU $= 10^{16}\ electrons/m^2$) extracted from phase/code observations at epoch t_p observed by receiver r and satellite s;
- $M(e_r^s)$: the mapping function that is used to project vertical TEC to slant TEC with respect to the elevation angle e_r^s;
- $a_{r,0}$, $a_{r,1}$, $a_{r,2}$: the ionospheric parameters to approximate the TEC spatial variation in linear form;
- $\triangle\lambda_r^s$: the geographic longitude of an ionospheric pierce point (IPP) referenced to the solar-geomagnetic coordinate system, i.e., the difference between the longitude of an IPP and the longitude of the mean sun;
- $\triangle\phi_r^s$: the difference between the geomagnetic latitude of the IPP and the geomagnetic latitude of the station;
- dcb_r: receiver instrumental bias, i.e., receiver DCB (TECU);
- dcb^s: satellite instrumental bias, i.e., satellite DCB (TECU);
- r: a ground GNSS receiver;
- s: a GNSS satellite.

The mapping function used in the model is the standard geometric mapping function [*Mannucci et al.*, 1993], which computes the secant of the zenith angle of the signal geometric ray path at the IPP at a shell height. Due to the dependence of the ionosphere on solar radiation and the geomagnetic field, the solar-geomagnetic reference frame is used to compute TEC over each station in this technique. Since the ionosphere changes more slowly in the Sun-fixed reference frame than in the Earth-fixed one, such a reference frame is ideal to produce more accurate TEC estimates [*Mannucci et al.*, 1995].

However, the initial version of UNB-IMT ignored the non-linear spatial variation of the ionosphere. Non-linear

terms are expected to be able to absorb more complex variability of the ionosphere and thus more properly describe the ionosphere in disturbed conditions. Regarding this issue, the drawbacks of some modelling methods were reported: e.g., the highly variable ionosphere might be absorbed by the estimated DCBs, making the repeatability of the estimated DCBs (day-to-day variability) correlated with the variability of the ionosphere [*Ma and Maruyama*, 2003; *Sardón and Zarraoa*, 1997; *Zhang et al.*, 2009]. To enhance the performance of UNB-IMT, especially under disturbed ionospheric conditions, *Rho et al.* [2004] extended the linear version of UNB-IMT to a quadratic one and assessed it by using a wide-area regional network in North America. This modified approach reduced the post-fit residuals significantly by better modelling the ionospheric variations with the help of the additional second order (non-linear) terms. The equation was expressed in the form:

$$\begin{aligned} TEC_r^s(t_p) = M(e_r^s)\cdot[a_{r,0}(t_p) + a_{r,1}(t_p)\cdot\triangle\lambda_r^s \\ +a_{r,2}(t_p)\cdot\triangle\phi_r^s + a_{r,3}(t_p)\cdot(\triangle\lambda_r^s)^2 + a_{r,4}(t_p)\cdot(\triangle\phi_r^s)^2 \\ +a_{r,5}(t_p)\cdot(\triangle\lambda_r^s\cdot\triangle\phi_r^s)] + dcb_r + dcb^s, \end{aligned} \quad (2)$$

where $a_{r,3}$, $a_{r,4}$, $a_{r,5}$ are the second order ionospheric parameters to approximate the TEC spatial variation in the non-linear form.

To better use the information provided by the IRI-2007 in the development of 3D UNB-IMT, we separate the TEC into a background reference part (a.k.a. known part) $TEC_{r,0}^s(t_p)$ and a perturbation part (a.k.a. to be modelled part) $\delta TEC_r^s(t_p)$

$$\begin{aligned} TEC_r^s(t_p) &= TEC_{r,0}^s(t_p) + \delta TEC_r^s(t_p) + dcb_r + dcb^s \\ &= \int_r^s N_{e,0}(\lambda,\phi,z,t_p)ds + \int_r^s \delta N_e(\lambda,\phi,z,t_p)ds \\ &\quad + dcb_r + dcb^s, \end{aligned} \quad (3)$$

where λ, ϕ, z represent geographic longitude, geomagnetic latitude, and height respectively, referenced to a solar-geomagnetic frame. $\int_r^s$ denotes the integration of the electron content along the line of sight from a GNSS satellite to a ground receiver. The background reference part of TEC ($TEC_{r,0}^s(t_p)$) could be calculated from any a priori source, such as any kind of ionospheric model, including empirical and theoretical ionospheric models.

Then, the perturbation part of electron density δN_e is modelled by the inner product of EOFs and polynomial functions to depict the variability of the ionosphere in the vertical and horizontal respectively. Take the model in quadratic form as an example:

$$\begin{aligned} \delta N_e(\lambda,\phi,z,t_p) = \sum_{k=1}^{K}\Big\{ a_{r,6k-5}(t_p)Z_k(z) \\ +a_{r,6k-4}(t_p)\triangle\lambda_r^s Z_k(z) + a_{r,6k-3}(t_p)\triangle\phi_r^s Z_k(z) \\ +a_{r,6k-2}(t_p)(\triangle\lambda_r^s)^2 Z_k(z) + a_{r,6k-1}(t_p)(\triangle\phi_r^s)^2 Z_k(z) \\ +a_{r,6k}(t_p)(\triangle\lambda_r^s\cdot\triangle\phi_r^s)Z_k(z)\Big\}, \end{aligned} \quad (4)$$

where $Z_k(z)$ is the EOF with K denoting the highest order of EOF; $a_{r,*}$ are the ionospheric parameters/coefficients to be estimated. Combining Equations 3 and 4, the observation equation of 3D UNB-IMT can then be established as

$$\begin{aligned} TEC_r^s(t_p) = TEC_{r,0}^s(t_p) + \sum_{k=1}^{K}\Big\{ a_{r,6k-5}(t_p)\int_r^s Z_k(z)ds \\ +a_{r,6k-4}(t_p)\int_r^s \triangle\lambda_r^s Z_k(z)ds + a_{r,6k-3}(t_p)\int_r^s \triangle\phi_r^s Z_k(z)ds \\ +a_{r,6k-2}(t_p)\int_r^s (\triangle\lambda_r^s)^2 Z_k(z)ds \\ +a_{r,6k-1}(t_p)\int_r^s (\triangle\phi_r^s)^2 Z_k(z)ds \\ +a_{r,6k}(t_p)\int_r^s (\triangle\lambda_r^s\cdot\triangle\phi_r^s)Z_k(z)ds\Big\} \\ +dcb_r + dcb^s. \end{aligned} \quad (5)$$

Equation 5 is the fundamental observation equation of 3D UNB-IMT, in which the number of coefficients depends on the order of polynomial functions we selected.

2. EOF

The EOF method is a method of choice for analyzing the variability of a single field (with only one scalar variable). Variability of the ionosphere with respect to height is needed for the 3D models. The method finds the spatial patterns of variability based on historical data sets. In other words, the modes of variability decomposed by the method are primarily "data modes", and not necessarily physical/actual models. Due to its remarkable performance for describing the background ionosphere [*Bilitza and Reinisch*, 2008], the data sets output from the empirical ionospheric model, IRI-2007, are utilized to form the EOF in this paper.

Thus, the data sets of electron densities are realized by uniform sampling at the specific geographic locations in the following variant time scale intervals:

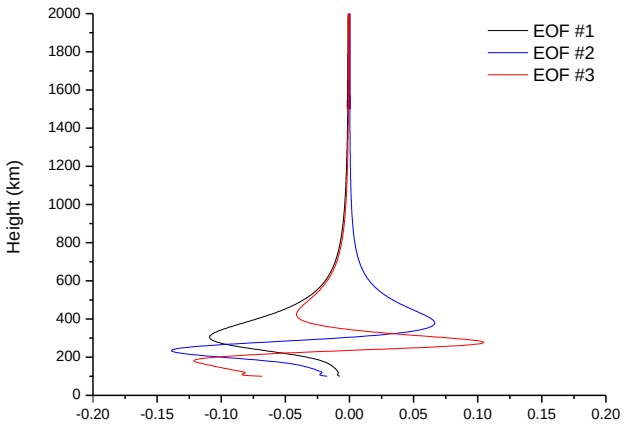

Figure 1: *The normalized first three dominant EOFs extracted from IRI-2007 empirical model*

- Solar cycle: [1998:1:2008] (year)
- Season of Year: [Dec, Mar, Jun, Sep] (month)
- Geographic latitude: [30°:5°:60°] (degree)
- Geographic longitude: [280°:5°:300°] (degree)
- Day time: [1:1:24] (hour)
- Day of month: [1:9:28] (day of month),

where the numbers separated by colon notations correspond to minimum:increment:maximum. The data sets cover the the whole area of interest. The data sets of a whole solar cycle in typical equinox and solstice months are used to ensure that the EOFs span the range of profile variations that include the variation in solar EUV output. Each electron density profile with respect to height at these locations at these sampled time points is sampled in the vertical dimension at [100:2:2000] (km). Figure 1 shows the first third order normalized EOFs based on the data sets. The first three eigenvalues account for 92.22%, 6.69%, 0.78% of the total respectively. Provided the solution is nonsingular, the choice of the highest order of EOFs is a trade off between processing time and modelling accuracy as to the specific network and capability of computer(s) [*Bjornsson and Venegas*, 1997]. In this paper, the highest order of 3 is chosen. In this case, the neglected vertical variation of the ionosphere corresponding to higher order EOFs is 0.31%.

Once the modelling approach has been constructed, the following task is to estimate the coefficients. Considering the potential real-time applications, a Kalman filter is employed to solve Equation 5. To be specific, the following settings are used. The correlation time is set to 5 minutes, which correspond to the WAAS update interval for ionospheric grid points. The uncertainty of the dynamic model, $0.008 TECU^2/second$, is chosen to characterize the rapid change of the ionosphere.

Finally, as long as the coefficients $a_{r,*}$ have been estimated through the Kalman filter, the ionospheric electron density field $N_e(\lambda,\phi,z,t_p)$ could be reconstructed by

$$\begin{aligned} N_e(\lambda,\phi,z,t_p) = N_{e,0}(\lambda,\phi,z,t_p) + \sum_{k=1}^{K} \Big\{ & a_{r,6k-5}(t_p) Z_k(z) \\ & + a_{r,6k-4}(t_p) \triangle\lambda_r^s Z_k(z) + a_{r,6k-3}(t_p) \triangle\phi_r^s Z_k(z) \\ & + a_{r,6k-2}(t_p) (\triangle\lambda_r^s)^2 Z_k(z) + a_{r,6k-1}(t_p) (\triangle\phi_r^s)^2 Z_k(z) \\ & + a_{r,6k}(t_p) (\triangle\lambda_r^s \cdot \triangle\phi_r^s) Z_k(z) \Big\}, \end{aligned} \tag{6}$$

where the $N_{e,0}(\lambda,\phi,z,t_p)$ indicates the a priori background electron density field (from IRI-2007 in this paper).

RESULTS

In this section, the 3D UNB-IMT is investigated and its performance is compared with that of the 3D SH approach. Due to the advantages of sensitivity of 2D UNB-IMT, especially with the single-station processing strategy [*Rho et al.*, 2005], it is expected that this technique will help in capturing localized ionospheric structures above small regional networks or above a single standalone station compared to the 3D SH approach. Additional benefits may be expected for disturbed ionospheric conditions.

For assessing the two modelling techniques, a small regional network of 4 IGS reference stations located from geographic latitude 39.0° N to 48.1° N and longitude 66.7° W to 77.6° W was chosen to perform single-station and multi-station (network) processing. Figure 2 shows the locations and distributions of the reference stations used for the modelling. The data used for the tests were observed from October 13-25 (day of year (DOY) 286-298) in 2011 with the sampling time interval of 30 seconds. The corresponding interplanetary magnetic field (IMF) B_z component, Kp index, AE index, Dst index on these days are shown in Figure 3. It is seen that a severe ionospheric storm triggered by a coronal mass ejection (CME) from the Sun happens late on October 24, 2011, and through the whole day of October 25, 2011. The other days are relatively quiet. Thus, we chose October 16, 2011, as the typical day with quiet iono-

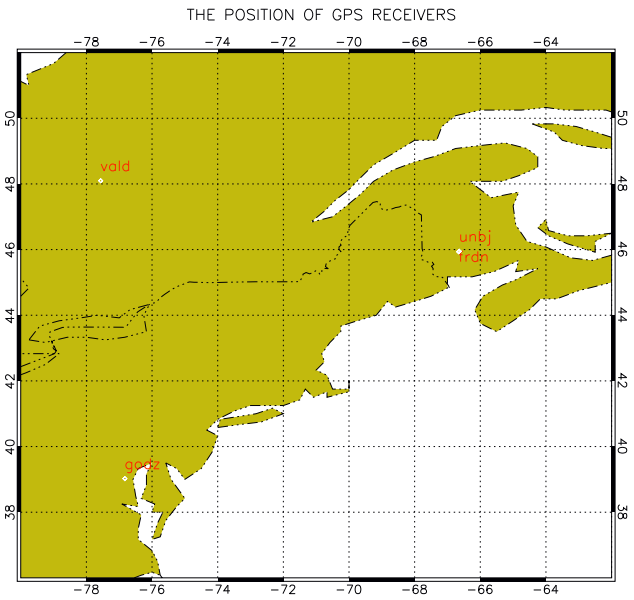

Figure 2: *The network of the four stations used in the evaluation procedures*

spheric conditions while October 25, 2011, as the typical day with disturbed ionospheric conditions in the following tests. The performance of both methods (3D UNB-IMT and SH model) with the two processing scenarios will be compared by analyzing the post-fit residuals and TEC of the state estimation process for both quiet and disturbed ionospheric conditions.

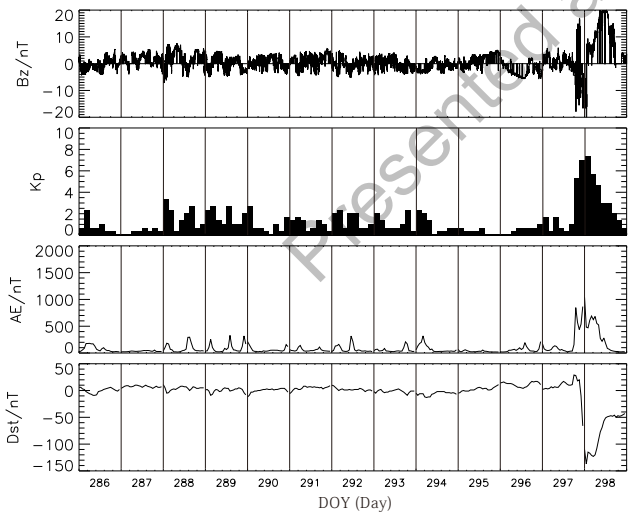

Figure 3: *Interplanetary magnetic field's B_z component, Kp index, AE index; Dst index on October 13-25 (DOY 286-298) in 2011 (Data from World Data Center for Geomagnetism, Kyoto and Goddard's Space Physics Data Facility)*

All 4 reference stations in the small network have the ability of providing both C and P code pseudo-range measurements. In the following tests, the P code observable is used to extract TEC through leveling carrier phase measurements. A 15° elevation cut-off angle is used in this study.

1. Single Station Experiment

As we have seen from Equation 3 and 4, the estimated parameters of 2D and 3D UNB-IMT have different physical meanings due to the different modelling strategies. In theory, the 3D UNB-IMT can reproduce the electron densities for any location (horizontal and vertical) at any epoch. Figure 4 shows an example of the electron density profile produced by the linear 3D UNB-IMT in the zenith direction of FRDN at 12:00 UT on October 16 (DOY 289), 2011. Therefore, we will have to integrate electron densities into TEC for the 3D UNB-IMT modelling results if we want to compare how the two approaches have modelled the ionosphere side by side. For the purpose of sensitivity comparison, the results from 2D and 3D UNB-IMT are compared in terms of post-fit residuals as well as time series of estimated vertical TEC in the single-station processing scenario. As discussed above, we use the GPS data from station FRDN only for October 16 and 25, 2011, in this subsection. The post-fit residuals are calculated as the difference between the measured and estimated biased slant TEC.

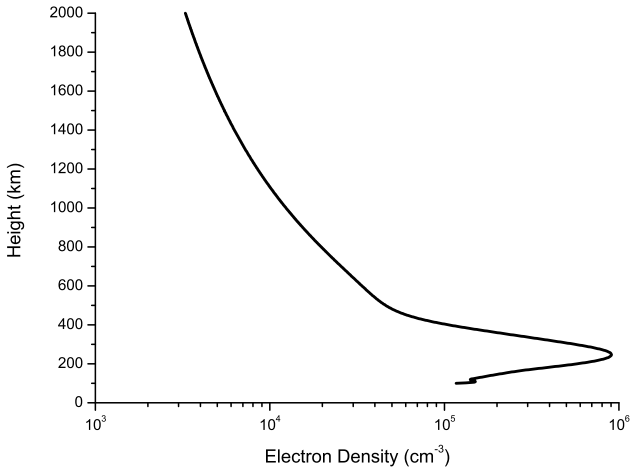

Figure 4: *The electron density profile produced by linear 3D UNB-IMT over head of FRDN at 12:00 (UT) on October 16 (DOY 289) in 2011*

From the top to bottom panels, Figure 5 shows the estimated vertical TEC in the zenith direction over the station, post-fit residuals, estimated satellite and receiver DCB, and unbiased slant TEC with respect to local mean solar time se-

ries obtained with linear 2D and 3D UNB-IMT approaches respectively. We use a different color for each satellite to see individual improvement of satellites in terms of post-fit residuals, estimated DCB, and unbiased slant TEC. As the potential improvement of 3D UNB-IMT we supposed, if the 2D model with single-shell assumption does not depict the variability of the ionosphere quite well (especially the vertical variability of the ionosphere), we should expect to see the improvement from the 3D model in terms of post-fit residuals. As seen in this figure, the 3D UNB-IMT improves the results in terms of post-fit residuals. The means and standard deviations of the residuals with the 2D and 3D UNB-IMT are shown in Table 1. The 3D UNB-IMT with three times more parameters is allowed to "accommodate" more (vertical) variations of the ionosphere. The benefits are also manifest in the improvement of the estimated vertical TEC and estimated satellite and receiver DCBs. In terms of estimated vertical TEC, the smooth variation of TEC may be expected at mid-latitudes during quiet ionospheric conditions without any ionospheric anomaly. The unmodelled variation of TEC in 2D UNB-IMT seen from post-fit residuals is also manifest as "artificial small jumps" in the vTEC panel. In other words, the 3D UNB-IMT is able to better "explain" the measurement from low-elevation-angle satellites owing to the EOFs replacing the mapping function. It is the typical case when a satellite comes into or goes out of view of the receiver. The estimated DCBs are relatively constant over the entire day. But it is also found from the estimated DCBs that the results from 2D UNB-IMT have slightly more variabilities. Both effects seem to be related to the unmodelled errors. The post-fit residuals in the 3D UNB-IMT are closer to the zero mean Gaussian distribution.

Then we further evaluated the performance of 2D and 3D UNB-IMT under significantly disturbed conditions. Figure 6 shows the results with the same modelling strategies as demonstrated in Figure 5 but on October 25, 2011. Similar conclusions can be drawn from Figure 6, where better results in terms of post-fit residuals are obtained with 3D UNB-IMT (Table 1). In terms of estimated vertical TEC, the results from both strategies in the disturbed condition look much more bumpy than those in the quiet condition and a little off the sine-wave-like daily variation. Some actual variation of the ionosphere during disturbed conditions may be captured and correctly illustrated as the bumps for both approaches. In the meanwhile, the unmodelled errors may also be explained as artificial small jumps/bumps in vTEC curves (revealed by the magnitude of post-fit residuals). It is seen that 3D linear UNB-IMT explains more variation of the ionosphere than 2D linear UNB-IMT. However, some residual unmodelled errors may still exist with the 3D model.

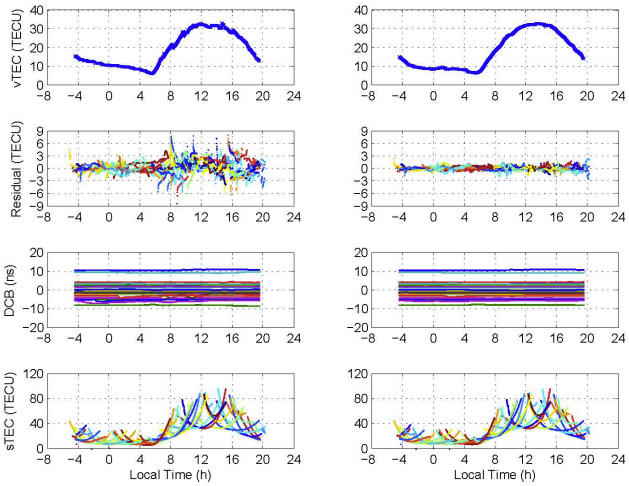

Figure 5: *Sensitivity test (the panels from the top to the bottom correspond to: estimated vertical TEC, post-fit residuals, satellite and receiver DCB, slant TEC with respect to local time series) between linear 2D (the left panels) and 3D (the right panels) models at FRDN on October 16 (DOY 289) in 2011.*

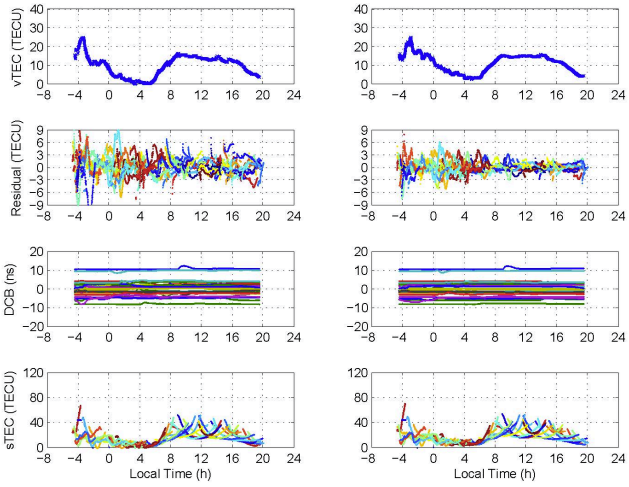

Figure 6: *Sensitivity test (the panels from the top to the bottom correspond to: estimated vertical TEC, residuals, satellite and receiver DCB, slant TEC with respect to local time series) between linear 2D (the left panels) and 3D (the right panels) models at FRDN on October 25 (DOY 298) in 2011.*

As concluded and demonstrated in *Rho et al.* [2004] and *Anghel et al.* [2009], a higher order model could explain

more spatial (non-linear) variations of the ionosphere, especially for the geomagnetic storm conditions. The results with 2D and 3D quadratic UNB-IMT approaches are shown in Figure 7. In the post-fit residual panels, it can be seen that the residuals with 3D quadratic UNB-IMT are mostly within ±2 TECU except for several small spikes that happened between 0:00 and 4:00 LT and reflect that not all the electron density variations had been correctly represented by the model used. But it is clear that the 3D quadratic UNB-IMT can significantly improve the modelling precision compared to the 2D quadratic/linear UNB-IMT and 3D linear UNB-IMT. The magnitude of the post-fit residuals shown in this panel is even comparable with the results in the quiet condition shown in Figure 5. In terms of vTEC, a few spurious spikes are occasionally found when processing the data from the 4 stations with the 3D quadratic model and single-station processing strategy. The other data sources, such as data from ionosondes, may be needed to confirm if the spikes are caused by the instability of the model or actual ionospheric structures. Still, the vTEC curves with 3D quadratic UNB-IMT look much smoother than 2D UNB-IMT. In terms of estimated DCBs, it is found that the results with 3D quadratic UNB-IMT approach exhibit relatively fewer perturbations than the other three approaches tested.

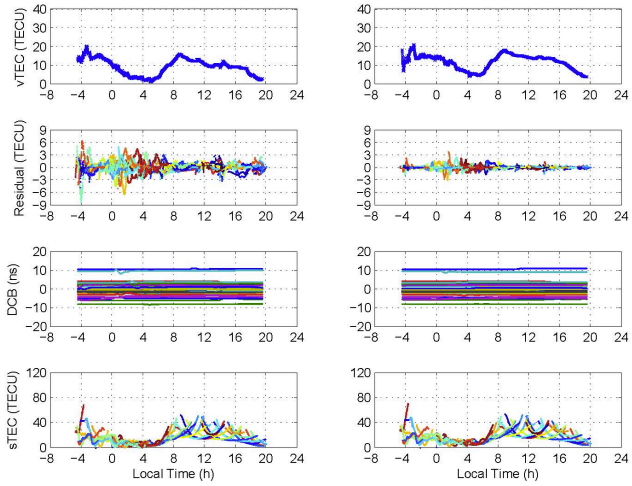

Figure 7: *Sensitivity test (the panels from the top to the bottom correspond to: estimated vertical TEC, residuals, satellite and receiver DCB, slant TEC with respect to local time series) between quatratic 2D (the left panels) and 3D (the right panels) models at FRDN on October 25 (DOY 298) in 2011.*

As we analyzed for the 2D modelling approaches, the single thin shell assumption with a fixed ionospheric shell height may introduce additional modelling errors. That is mainly because the layer with highest electron density (F2 layer) is not always located at a fixed height. Especially in disturbed ionospheric conditions, such as the case shown in Figure 6 and Figure 7, the layer height would change significantly. Some methods were proposed and tested with the help of more reliable "true" heights from other resources, such as ionosonde [*Garcia-Fernandez*, 2004; *Komjathy*, 1997; *Lee*, 2007; *Mushini et al.*, 2009]. However, due to limited number of the instruments deployed and limited information (only information from over head) provided, the applications with these methods would have to be limited to the specific area covered by stations or networks equipped with the instruments. In addition, as to real-time application, the data processing time delay of ionosondes might be another technical issue these methods have to face. Compared with these methods, one benefit of the 3D UNB-IMT is its potential for real-time application for any size of network. Another benefit is its vertical modelling capability to depict vertical variation of electron density so the improved results would also be expected for disturbed ionospheric conditions. It is clearly seen from Figure 6 and Figure 7 that the lowest vTECs around 4:00 LT reach down to 0 TECU with the 2D linear/quatratic UNB-IMT, which are considered as unphysical results. It is confirmed that small biases still exist in the results with the 2D model likely due to the improper shell height chosen (fixed at 350 km in this paper).

Table 1: *The means and standard deviations of the residuals under the quiet (Oct. 16th, 2011) and disturbed (Oct. 25th, 2011) ionospheric conditions*

U TECU	M (2D)	SD (2D)	M (3D)	SD (3D)
L (Q)	0.217	1.450	0.021	0.440
L (S)	0.077	2.107	0.011	1.256
Q (S)	0.047	1.125	0.006	0.376

2. Multi-station Experiment

When using the modelling scheme for a network solution, we may generally have two possible processing scenarios. One is processing the data of all the stations as a batch, and the other is processing station by station (or baseline by baseline as implemented in *Komjathy* [1997] and *Rho et al.* [2004]).

The advantages and disadvantages of the batch process can be summarized as follows. It has more redundancies in the Kalman filter to estimate a more stable and reliable set of satellite and receiver DCBs. Due to more measurements

as an input (state) of the Kalman filter, the convergence time would be shorter in terms of the estimated DCBs. It would be of benefit for real-time application if we have limited a priori information about the estimated ionospheric parameters and/or DCBs. However, the batch solution seems to be less sensitive to localized information content than the station-by-station solution. The overall effect of the batch solution is smoothing over the network, reducing the size of some small perturbations. Theoretically, localized measurements should not have significant influence on the estimated state across an extended area or even the entire globe. In other words, the batch solution may be beneficial for relatively small local-area networks, but may not be ideally suited for networks as large as wide-area networks. *Rho et al.* [2005] did significant work with 2D UNB-IMT and a wide-area WAAS-like network and reached similar conclusions. Another straightforward disadvantage of the batch process is its relatively longer processing time, which might be a downside if it is used for real-time applications.

Table 2: *Baseline distances between the GPS stations in the selected network (km)*

	FRDN	GODZ	UNBJ	VALD
FRDN	0	1132	2	860
GODZ	1132	0	1135	1011
UNBJ	2	1135	0	861
VALD	860	1011	861	0

In this multi-station experiment, we test the 3D UNB-IMT with a small regional network of 4 IGS reference stations (Figure 2) to investigate its performance with ionospheric localized variations. As we analyzed above, the difference of sensitivities between batch and station-by-station solutions might be less with the shorter baselines of the network. Therefore, we selected 3 stations with moderate length of baselines (about 1000 km), which are also comparable with the moderate length of baselines of WAAS reference stations, to see the difference of sensitivities. We also selected one more station which is close to one of the three stations for validation purposes. The baseline separations between any two stations are given in Table 2.

For assessing the 3D UNB-IMT with the network, the tests were performed with two scenarios: batch and station-by-station processes. The performance of 2D and 3D UNB-IMT with the two processing scenarios is compared in this subsection. To be specific, the data from all four reference stations was processed according to these strategies. We

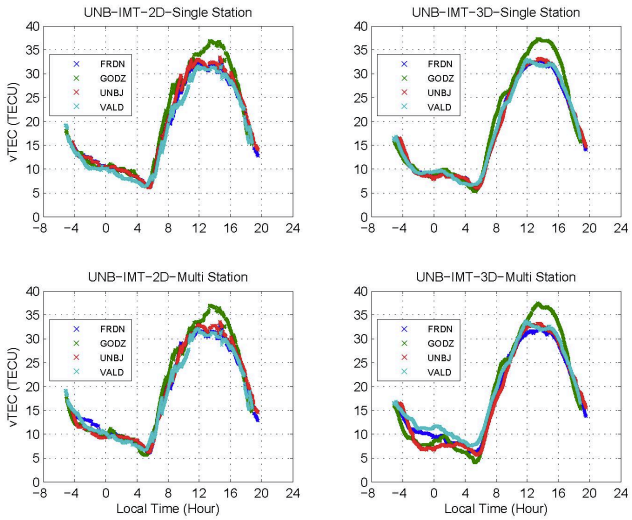

Figure 8: *Estimated vertical TEC in the zenith direction of the stations by using different processing strategies for the data collected on October 16 (DOY 289) in 2011: linear 2D model with single station (upper-left panel); linear 3D model with single station (upper-right panel); linear 2D model with multi-station (lower-left panel); linear 3D model with multi-station (lower-right panel).*

will expect the vTECs from FRDN and UNBJ stations to be nearly the same in both processing scenarios, especially for quiet ionospheric conditions if the modelling approaches and processing strategies model the ionosphere properly.

Similar to the results seen in the figures in the last subsection, the improvement in terms of post-fit residuals is also seen in the multi-station tests. We show the estimated vertical TEC overhead for the tests in this subsection as large residuals can also be manifest as "artificial jumps" in vTEC as seen in the results of the single-station tests.

Figure 8 displays the estimated vertical TEC in the zenith direction of the stations for the selected 4 stations obtained with the 2D single-station, 2D multi-station, 3D single-station, 3D multi-station UNB-IMT processing strategies for October 16 (DOY 289) in 2011. It is illustrated in the left two panels that "artificial small jumps" are found when a satellite comes into view at a low elevation angle for both batch and station-by-station processing scenarios. Comparing these results, the vTEC curves with respect to local time in the right two panels look much smoother. As with the conclusion drawn from the single-station test, the 3D UNB-IMT with EOFs seems to be able to better model the measurements with low elevation angles than the 2D UNB-IMT with a mapping function. By comparing the

vTEC curves for FRDN and UNBJ indicated by blue and red colors, we can see their corresponding results in the upper two panels do nearly overlap each other, indicating that the models do perform well in the estimation of DCBs and the station-by-station processing strategy is free from any impacts of the measurements from the other stations. On the other hand, the results for FRDN and UNBJ with the batch process shown in the lower two panels deviate slightly during some periods of time. The unreasonable results with the batch process are considered as a side effect of the adjustment of the ionospheric parameters among all 4 stations. The resulting effect of the batch process tends to be making the overall ionosphere smoother. As well, a more unrealistic interpretation of the variability of the ionosphere appears.

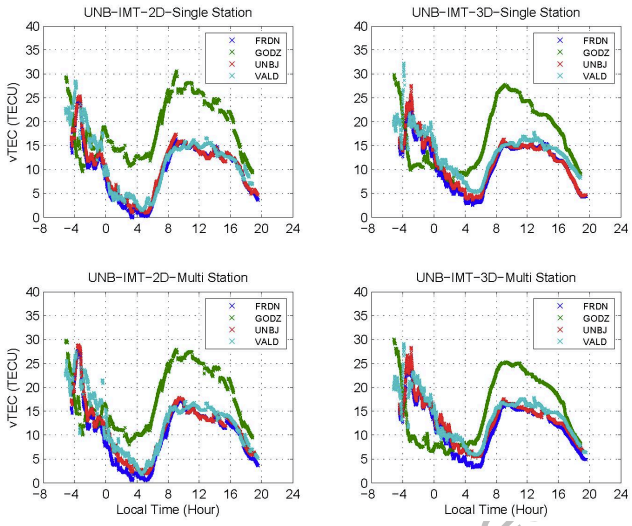

Figure 9: *Estimated vertical TEC in the zenith direction of the stations by using different processing strategies for the data collected on October 25 (DOY 298) in 2011: linear 2D model with single station (upper-left panel); linear 3D model with single station (upper-right panel); linear 2D model with multi-station (lower-left panel); linear 3D model with multi-station (lower-right panel).*

Then, we further tested the linear 2D and 3D UNB-IMT with the data on October 25 (DOY 298) in 2011. Figure 9 shows the vTEC curves with the same processing scenarios and modelling strategies as Figure 8 but on October 25, 2011. Similar conclusions about the benefit of 3D UNB-IMT can be drawn from Figure 9. But the "artificial jumps" due to the errors from the mapping function look more significant, implying that the thin-shell assumption does not hold well for low-elevation-angle measurements under disturbed ionospheric condition. By comparing the results of the station-by-station and batch processes with 3D UNB-IMT, the vTECs from FRDN and UNBJ overlap very well. It can also be noticed and confirmed that the vTEC from GODZ located at a lower latitude, from which larger TEC is observed, still have unmodelled biases in the batch processing. It also manifests the downside of UNB-IMT to process the data of long-baseline networks with so-called data gaps in the batch solution. For obtaining better reconstruction of the ionosphere, the results in the tests seem to suggest the station-by-station solution with 3D UNB-IMT is better.

As to the estimated DCBs with 2D UNB-IMT, the unreal fixed shell height assumption and complex electron density distribution during the ionospheric storm leads to less accurate estimated DCBs, seen as zero vTEC in the left panels of Figure 9. The accuracy of estimated DCBs under disturbed ionospheric conditions is a critical issue for improving the accuracy of ionospheric modelling. As a downside of 2D UNB-IMT on this issue, some other modelling techniques were also demonstrated to have the same problem [*Zhang et al.*, 2009]. The performance of the estimation of DCBs by the 3D UNB-IMT under disturbed conditions is worth evaluating thoroughly in future works.

It has been concluded that processing strategies, such as station-by-station and batch processing, may impact the accuracy of estimated DCBs. Choosing one or the other processing strategy is a tradeoff issue. The batch solution provides more stable estimation of DCBs owing to the larger number of measurements fed per state. But it also has an averaging effect on the reconstructed ionosphere, which might further decrease the accuracy of estimated DCBs, such as the difference of vTEC at GODZ with station-by-station and batch processing strategies. The evaluation of the accuracy of the estimated DCBs with the 3D UNB-IMT with both processing strategies is out of scope of the paper. However, the benefits of the 3D UNB-IMT on the potential improvement of the repeatability of estimated DCBs will be shown in the last subsection.

Furthermore, tests were also performed with 2D and 3D quadratic UNB-IMT approaches and the data observed during disturbed ionospheric conditions. Similar conclusions can be drawn from the comparison between the two processing strategies.

3. Comparing 3D UNB-IMT with SH Model

As we have seen from the comparison between batch and station-by-station solutions, the station-by-station scheme is more sensitive to localized variability. On the other hand,

in the following experiment, we compromised on the sensitivity of the solution and used the batch processing scheme. Subsequently, we compared the results with this strategy with those from the SH model. The reason for this approach is that we intend to compare the results of the two processing strategies (UNB-IMT and SH) with identical conditions. That is, both methods will process the data using a batch scheme and estimate both ionospheric parameters and DCBs simultaneously, instead of using some other source or processed results. Therefore, in this case, we can compare the results side by side and evaluate the effectiveness of the estimated ionospheric parameters.

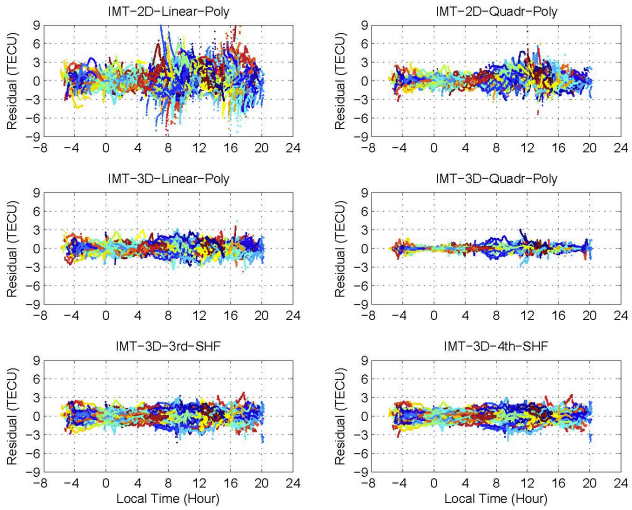

Figure 10: *Residuals of batch processing for data collected on October 16 (DOY 289), 2011, with different modelling strategies: linear 2D polynomial model (upper-left panel); quadratic 2D polynomial model (upper-right panel); linear 3D polynomial model (mid-left panel); quadratic 3D polynomial model (mid-right panel); up to the third order spherical harmonic 3D model (lower-left panel); up to the fourth order spherical harmonic 3D model (lower-right panel)*

Figure 10 shows the batch solutions for October 16, 2011, with different modelling strategies. As labeled on top of each panel, the modelling strategies include: linear 2D UNB-IMT, quadratic 2D UNB-IMT, linear 3D UNB-IMT, quadratic 3D UNB-IMT, up to third order 3D SH model, up to fourth order 3D SH model. These particular highest orders of SH model were selected as the number of ionospheric parameters to be estimated with them are comparable with the tested 3D UNB-IMT model. The corresponding number of ionospheric parameters to be estimated is 12, 24, 36, 72, 48, 75 for the 6 modelling strategies. The corresponding mean and standard deviation of the post-fit residuals are listed in Table 3. The improvement of the sensitivity of 3D UNB-IMT is confirmed by the post-fit residuals. Based on the data from the network of the 4 stations with such baselines, the sensitivity of the SH models is lower than that of 3D UNB-IMT, although the number of ionospheric parameters of the SH models is comparable or even larger than that of 3D UNB-IMT. In other words, the ionospheric parameters in 3D UNB-IMT to describe the variability of the ionosphere are more effective and meaningful to such a network scale than those in the 3D SH model.

Table 3: *The mean and standard deviation of the post-fit residuals for the two selected days, October 16 and 25 (DOY 289 and 298) , 2011, with quiet and disturbed ionospheric condition respectively*

Unit:	Quiet (Oct. 16)		Storm (Oct. 25)	
(TECU)	Mean	St. Dev.	Mean	St. Dev.
L 2D UNB	0.126	1.806	0.029	2.656
Q 2D UNB	0.051	0.895	0.012	1.301
L 3D UNB	0.012	0.960	0.011	2.003
Q 3D UNB	-0.001	0.351	-0.001	0.543
3D SH 3rd	-0.008	0.978	-0.006	1.935
3D SH 4th	-0.007	0.906	-0.009	1.658

Given the nature of its basis functions, the SH model is an excellent tool for global modelling except for some shortcomings for localized variability modelling [*Li*, 1999; *Schmidt et al.*, 2008]. But it was also demonstrated that it could be implemented with a regional network, especially a wide-area regional network [*Allain and Mitchell*, 2009; *Liu et al.*, 2006]. As to larger regional networks with longer baselines, such as WAAS, which covers North America, the difference of the sensitivities between the batch solutions and the station-by-station should be larger than the results shown in this work. However, we cannot conclude that the sensitivity of 3D UNB-IMT is better than that of 3D SH model with batch processing strategy for such large regional networks here before more tests are conducted. Still, it is clearly seen in the tests that the 3D SH model is not always ideal for regional networks in terms of sensitivity.

Similar conclusions may be reached from Figure 11 for October 25 in 2011, where the residuals spread more widely compared with quiet-condition residuals. In the storm conditions, the residuals of the quadratic 3D UNB-IMT spread relatively less than those of other modelling strategies. This is especially the case for the several hours at the beginning of the day, which corresponds to the peak of Dst and Kp indices shown in Figure 3. The statistics, the mean and standard deviation, of the residuals in the

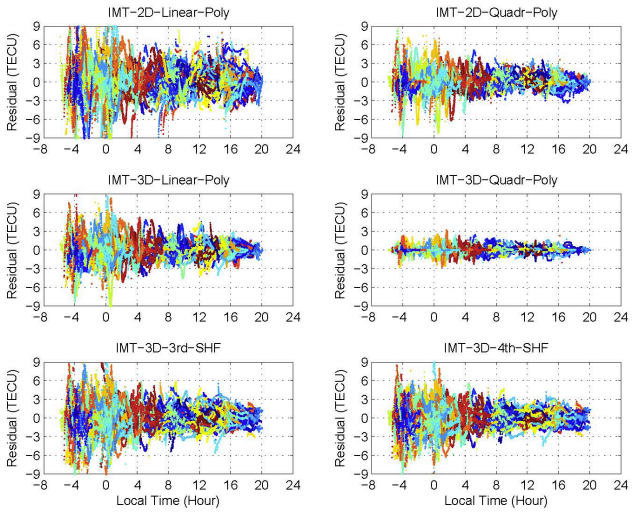

Figure 11: *Residuals of batch processing for data collected on October 25 (DOY 298), 2011, with different modelling strategies: linear 2D polynomial model (upper-left panel); quadratic 2D polynomial model (upper-right panel); linear 3D polynomial model (mid-left panel); quadratic 3D polynomial model (mid-right panel); up to the third order spherical harmonic 3D model (lower-left panel); up to the fourth order spherical harmonic 3D model (lower-right panel)*

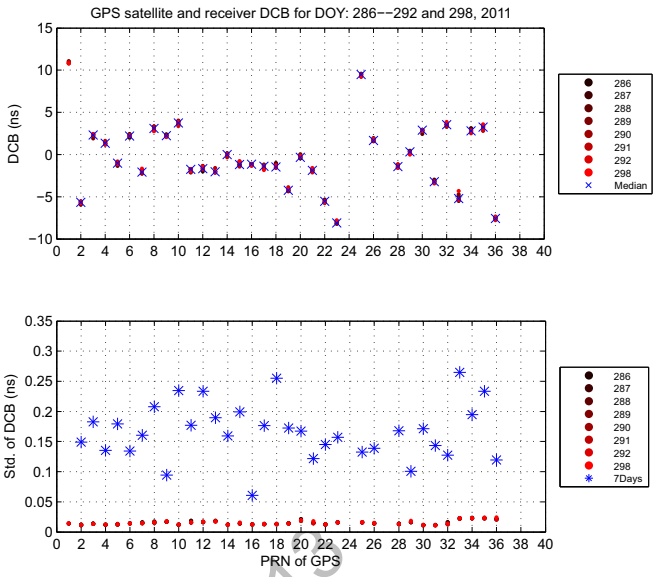

Figure 12: *Estimated GPS satellite and receiver DCBs (upper panel) with quadratic 2D polynomial model (2D UNB-IMT) for October 13-19 and 25 (DOY 286-292 and 298), 2011 and standard deviation of DCBs for the 7 days in quiet ionospheric conditions (lower panel)*

modelling strategies are given in Table 3. So the quadratic 3D UNB-IMT seems to have the capacity to handle the ionospheric spatial and temporal variation even in the severe storm condition.

4. Repeatability of Estimated DCBs

The DCBs not only have influence on the quality (accuracy) of the VTEC estimation, but its repeatability can also provide information to evaluate ionospheric models. This implies that the ionospheric models that have the capability to estimate/eliminate more accurate DCBs, e.g. independent from the ionospheric variability, are preferable. In this subsection, the repeatability of DCBs estimated with 3D UNB-IMT is evaluated and compared with that with 3D SH model. It should be noted that the four stations used in the test can log both P1 and C/A code. In the evaluation, only P1 code is used, so the DCBs mean P1-P2 DCBs.

All satellite and receiver DCBs are relative biases. Should all satellite DCBs shift by a common bias, the bias would be absorbed by receiver DCBs. Usually a particular satellite or receiver can be chosen as reference, e.g. last version of 2D UNB-IMT, or all DCBs can be related to the mean of all satellite DCBs, which is considered as a more reliable constant value. In this version of UNB-IMT, including both 2D and 3D implementations, the latter is performed.

Figure 12 shows the DCB results with quadratic 2D UNB-IMT. The upper panel of the figure shows the daily estimated DCBs (colored dots) for October 13-19 and 25, 2011 with respect to satellite PRN number. The numbers 33-36 correspond to the receiver FRDN, GODZ, UNBJ, and VALD. The median (crosses) of DCBs for the seven quiet days (October 13-19) are also indicated in this panel. The lower panel gives the information of standard deviations of estimated DCBs. The standard deviations of DCBs for the seven quiet days are indicated by stars. The corresponding formal precisions with respect to satellite and receiver number are drawn as colored dots. The PRN01 satellite could only be observed on October 15-19, so it was not included in the processing of calculation of means and standard deviations for each satellite and receiver.

The corresponding results similar to the one with quadratic 2D UNB-IMT method but with different modelling strategies are shown in Figure 13 (quadratic 3D UNB-IMT) and Figure 14 (up to 3rd order 3D SH model). To assess the performance of 2D/3D UNB-IMT and 3D SH model for DCB estimation for both quiet and disturbed ionospheric

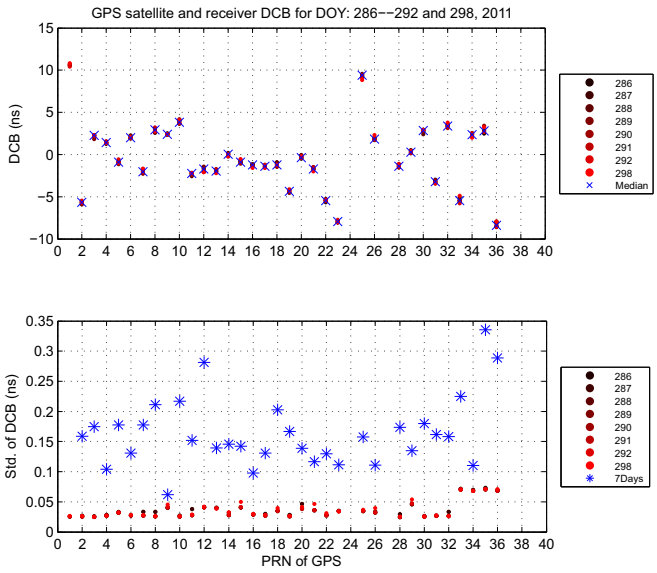

Figure 13: *Estimated GPS satellite and receiver DCBs (upper panel) with quadratic 3D polynomial model (3D UNB-IMT) for October 13-19 and 25 (DOY 286-292 and 298), 2011 and standard deviation of DCBs for the 7 days in quiet ionospheric conditions (lower panel)*

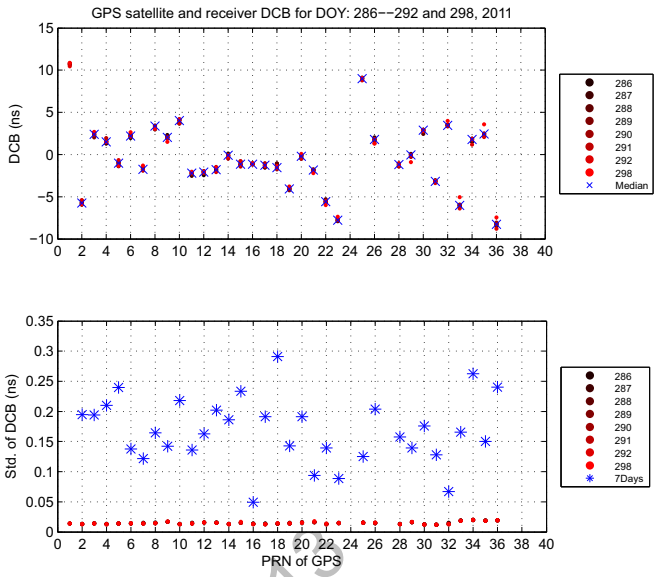

Figure 14: *Estimated GPS satellite and receiver DCBs (upper panel) with up to the third order 3D spherical harmonic model (3D SH) for October 13-19 and 25 (DOY 286-292 and 298), 2011 and standard deviation of DCBs for the 7 days in quiet ionospheric conditions (lower panel)*

conditions, the mean of the standard deviations of estimated DCBs for all the satellites and receivers ($\overline{\sigma}_{DCB(01-36)}$) is introduced. $\overline{\sigma}_{DCB(01-36)}(8)$ (for October 13-19 and 25) is chosen as an indicator of the performance of DCB estimation in disturbed ionospheric condition, while $\overline{\sigma}_{DCB(01-36)}(7)$ (for October 13-19 only) is for quiet conditions.

Table 4 summarizes the statistics. L indicates linear and Q stands for quadratic in this table. For the quiet conditions, it seems the smooth and light variability of the ionosphere can be represented adequately by all the modelling methods, although 3D UNB-IMT performs slightly better in terms of the repeatability of estimated DCBs. For the disturbed conditions, the benefit of quadratic 3D UNB-IMT is clearly seen in comparison with linear 2D/3D UNB-IMT and 3D SH model. The improvement of the models extended from 2D to 3D is slight for the quadratic models, although it is significant for the linear models. The performance of UNB-IMT with more effective and meaningful parameters is confirmed for the regional modelling in comparison with SH model.

Table 4: *The mean of the standard deviations of the estimated DCBs for all the satellites and receivers for the selected seven (October 13-19) and eight (October 13-19 and 25) days*

Unit: (ns)	L 2D	Q 2D	L 3D	Q 3D	3D SH
$\overline{\sigma}_{DCB(01-36)}(8)$	0.236	0.177	0.199	0.176	0.211
$\overline{\sigma}_{DCB(01-36)}(7)$	0.170	0.166	0.176	0.164	0.168

Conclusions and Future Research

In this paper, we extended the UNB-IMT from 2D to 3D and compared the performance between them in station-by-station and batch processing scenarios for both quiet and storm ionospheric conditions. We used the data from a small regional network of dual-frequency GPS receivers. The DCBs and ionospheric delays were estimated at the same time by the Kalman filter. The newly developed approach was evaluated by analyzing the post-fit residuals, TEC of the state estimation process, and the repeatability of estimates of DCBs.

As to the single-station processing, the improvement of 3D UNB-IMT has been demonstrated in both quiet and disturbed ionospheric conditions in terms of post-fit residuals. The 3D UNB-IMT with more parameters allows the depiction of more complex (vertical) variability of the ionosphere. The 3D UNB-IMT is able to better deal with the

measurements from low-elevation-angle satellites owing to EOFs replacing the mapping function. The "artificial jumps" with 2D UNB-IMT when satellites come into or go out of view of the receiver have been properly handled by the 3D UNB-IMT. In the meanwhile, the time series of estimated DCBs with 3D UNB-IMT exhibit less perturbation than the results with 2D UNB-IMT.

As to the multi-station (network) processing, it is confirmed that the station-by-station solution is more sensitive to localized information than the batch solution. By comparing the results from 3D UNB-IMT and 3D SH models with a comparable number of ionospheric parameters, we found that the sensitivity of the SH model is lower than that of 3D UNB-IMT for the regional network. The ionospheric parameters in 3D UNB-IMT to describe the variability of the ionosphere are more effective and meaningful to the regional network than those in the 3D SH model. Based on the results in this research, station-by-station processing with 3D UNB-IMT is suggested to increase chances to catch localized ionospheric structures.

The repeatability of estimated DCBs is investigated as another indicator to evaluate the ionospheric models. For the quiet ionospheric conditions, the performance of all the tested models looks comparable, although quadratic 3D UNB-IMT performs slightly better than the others. As to the disturbed conditions, the quadratic 2D/3D UNB-IMT seems be able to provide more stable DCBs than the other models. However, the improvement of the extension from 2D to 3D is slight for the quadratic models, although it is significant for the linear models. The performance of 3D SH model looks fairly poor compared to 3D UNB-IMT for the regional modelling.

Before the 3D UNB-IMT is tested in the positioning domain for single-frequency positioning, it is worth validating the model with other data sources. In addition, the potential benefits of 3D UNB-IMT during extreme disturbed ionospheric conditions is worth investigating further.

ACKNOWLEDGMENTS

We would like to thank the Crustal Dynamics Data Information System (CDDIS) for providing the GPS data and acknowledge the financial contribution of the Natural Sciences and Engineering Research Council of Canada (NSERC) to support the first and second authors.

REFERENCE

Allain, D. J., and C. N. Mitchell (2009), Comparison of 4D tomographic mapping versus thin-shell approximation for ionospheric delay corrections for single-frequency GPS receivers over North America, *GPS Solutions*, *14*(3), 279–291, doi:10.1007/s10291-009-0153-0.

Anghel, A., C. Carrano, A. Komjathy, A. Astilean, and T. Letia (2009), Kalman filter-based algorithms for monitoring the ionosphere and plasmasphere with GPS in near-real time, *Journal of Atmospheric and Solar-Terrestrial Physics*, *71*(1), 158–174, doi: 10.1016/j.jastp.2008.10.006.

Austen, J., S. Franke, and C. Liu (1988), Ionospheric imaging using computerized tomography, *Radio Science*, *23*(3), 299–307.

Bilitza, D., and B. Reinisch (2008), International Reference Ionosphere 2007: Improvements and new parameters, *Advances in Space Research*, *42*(4), 599–609, doi:10.1016/j.asr.2007.07.048.

Bjornsson, H., and S. Venegas (1997), A manual for EOF and SVD analyses of climatic data, *Tech. rep.*, Department of Atmospheric and Oceanic Sciences and Centre for Climate and Global Change Research, McGill University.

Feltens, J. (2007), Development of a new three-dimensional mathematical ionosphere model at European Space Agency/European Space Operations Centre, *Space Weather*, *5*(12), S12,002, doi:10.1029/2006SW000294.

Gao, Y., and Z. Liu (2002), Precise ionosphere modeling using regional GPS network data, *Journal of Global Positioning Systems*, *1*(1), 18–24.

Garcia-Fernandez, M. (2004), Contributions to the 3D ionospheric sounding with GPS data, Ph.D. thesis, Research group of Astronomy and Geomatics, Universitat Politècnica de Catalunya, Spain.

Hansen, A. (1998), Real-time ionospheric tomography using terrestrial GPS sensors, in *Proceedings of the 11th International Technical Meeting of the Satellite Division of The Institute of Navigation (ION GPS 1998)*, Nashville, TN, 15-18 September, 1998, pp. 717–727.

Hansen, A. (2002), Tomographic estimation of the ionosphere using terrestrial GPS sensors, Ph.D. thesis, Department of Electrical Engineering, Stanford University, Stanford, California, USA.

Hernández-Pajares, M., J. Juan, and J. Sanz (1999), New approaches in global ionospheric determination using ground GPS data, *Journal of Atmospheric and Solar-Terrestrial Physics*, *61*, 1237–1247.

Howe, B. M., K. Runciman, and J. a. Secan (1998), Tomography of the ionosphere: Four-dimensional simulations, *Radio Science*, *33*(1), 109–128, doi: 10.1029/97RS02615.

Komjathy, A. (1997), Global ionospheric total electron content mapping using the Global Positioning System, Ph.D. thesis, Department of Geodesy and Geomatics Engineering, University of New Brunswick, Fredericton, New Brunswick, Canada.

Komjathy, A., and R. Langley (1996a), An assessment of predicted and measured ionospheric total electron content using a regional GPS network, in *Proceedings of the 1996 National Technical Meeting of The Institute of Navigation*, Santa Monica, CA, 22-24 January 1996, pp. 615–624.

Komjathy, A., and R. Langley (1996b), Improvement of a global ionospheric model to provide ionospheric range error corrections for single-frequency GPS users, in *Proceedings of the 52nd Annual Meeting of The Institute of Navigation*, Cambridge, MA, 22-24 January 1996, pp. 557–566.

Lee, J. K. (2007), 3D Tomographic Imaging of the Ionosphere Using Global Positioning System Measurements, Ph.D. thesis, Department of Electrical and Computer Engineering, University of Illinois at Urbana-Champaign, Urbana, Illinois, USA.

Lee, J. K., F. Kamalabadi, and J. J. Makela (2007), Localized three-dimensional ionospheric tomography with GPS ground receiver measurements, *Radio Science*, *42*(4), doi:10.1029/2006RS003543.

Li, T.-H. (1999), Multiscale Representation and Analysis of Spherical Data by Spherical Wavelets, *SIAM Journal on Scientific Computing*, *21*(3), 924–953, doi: 10.1137/S1064827598341463.

Liu, Z., S. Skone, and Y. Gao (2006), Assessment of ionosphere tomographic modeling performance using GPS data during the October 2003 geomagnetic storm event, *Radio Science*, *41*(1), doi:10.1029/2004RS003236.

Ma, G., and T. Maruyama (2003), Derivation of TEC and estimation of instrumental biases from GEONET in Japan, *Annales Geophysicae*, *21*, 2083–2093.

Mannucci, A., B. Wilson, and C. Edwards (1993), A New Method for Monitoring the Earth's Ionospheric Total Electron Content Using the GPS Global Network, in *Proceedings of the 6th International Technical Meeting of the Satellite Division of The Institute of Navigation (ION GPS 1993)*, Salt Lake City, UT, 22-24 September 1993, pp. 1323–1332.

Mannucci, A., B. Wilson, D. Yuan, C. Ho, U. Lindqwister, and T. Runge (1998), A global mapping technique for GPS-derived ionospheric total electron content measurements, *Radio Science*, *33*(3), 565–582.

Mannucci, J. J., B. D. Wilson, and D.-N. Yuan (1995), An improved ionospheric correction method for Wide-Area Augmentation Systems, in *Proceedings of the 8th International Technical Meeting of the Satellite Division of The Institute of Navigation (ION GPS 1995)*, Palm Springs, CA, 12-15 September 1995, pp. 1199–1208.

Mitchell, C., and P. Spencer (2003), A three-dimensional time-dependent algorithm for ionospheric imaging using GPS, *Annals of Geophysics*, *46*(4), 687–696.

Mushini, S. C., P. Jayachandran, R. Langley, and J. MacDougall (2009), Use of varying shell heights derived from ionosonde data in calculating vertical total electron content (TEC) using GPS New method, *Advances in Space Research*, *44*(11), 1309–1313, doi: 10.1016/j.asr.2009.07.015.

Rho, H., R. Langley, and A. Komjathy (2004), An enhanced UNB ionospheric modeling technique for SBAS: The quadratic approach, in *ION GNSS 2004*, pp. 354–365.

Rho, H., R. Langley, and A. Komjathy (2005), SBAS ionospheric modeling with the quadratic approach: Reducing the risks, in *Proceedings of the 18th International Technical Meeting of the Satellite Division of The Institute of Navigation (ION GNSS 2005)*, Long Beach, CA, 13-16 September 2005, pp. 723–734.

Sardón, E., and N. Zarraoa (1997), Estimation of total electron content using GPS data: How stable are the differential satellite and receiver instrumental biases?, *Radio science*, *32*(5), 1899–1910.

Schaer, S., W. Gurtner, and J. Feltens (1998), IONEX: The IONosphere map eXchange format version 1, in *Proceedings of the IGS Analysis Center Workshop*, pp. 233–247.

Schmidt, M., D. Bilitza, C. Shum, and C. Zeilhofer (2008), Regional 4-D modeling of the ionospheric electron

density, *Advances in Space Research*, *42*(4), 782–790, doi:10.1016/j.asr.2007.02.050.

Sparks, L., J. Blanch, and N. Pandya (2011a), Estimating ionospheric delay using kriging: 1. Methodology, *Radio Science*, *46*(1), RS0D21, doi:10.1029/2011RS004667.

Sparks, L., J. Blanch, and N. Pandya (2011b), Estimating ionospheric delay using kriging: 2. Impact on satellite-based augmentation system availability, *Radio Science*, *46*(5), RS0D22, doi:10.1029/2011RS004781.

Wen, D., Y. Yuan, J. Ou, X. Huo, and K. Zhang (2007), Three-dimensional ionospheric tomography by an improved algebraic reconstruction technique, *GPS Solutions*, *11*(4), 251–258, doi:10.1007/s10291-007-0055-y.

Zhang, W., D. Zhang, and Z. Xiao (2009), The influence of geomagnetic storms on the estimation of GPS instrumental biases, *Annales Geophysicae*, *27*(4), 1613–1623.